Available online at www.sciencedirect.com
ScienceDirect
Trans. Nonferrous Met. Soc. China 33(2023) 2417−2427
Transactions of Nonferrous Metals Society of China
www.tnmsc.cn

Microstructure and mechanical property of bonding zones between Ta foil and steel plate fabricated by explosive welding

Ming YANG, Jin-xiang WANG

National Key Laboratory of Transient Physics, Nanjing University of Science and Technology, Nanjing 210094, China

Received 12 March 2022; accepted 26 July 2022

Abstract: This work aims to produce a thorough comprehension concerning microstructure related properties of the joint interface between Ta foil and steel plate fabricated by explosive welding. For this, a self-developed explosive welding configuration was employed to join Ta foil and steel plate, and different microscopic methods were adopted to investigate its microstructures and mechanical properties. It was found that the Ta/Fe interface was featured by regular wavy structures with a well-defined amplitude and period. The melted zones were mainly observed within the vortex structures, and occasionally at the Ta/Fe interfaces, which were formed by intense mixing of participating metals. The EBSD analyses revealed a diversity of the grain structures near the Ta/Fe interface, such as formation of the curved and elongated grains in Ta matrix, and fine equiaxed and columnar grains in Fe matrix. Especially, several adiabatic shear bands (ASBs) characterized by small equiaxed grains were found in Fe matrix, which were due to stress wave concentration in the narrow paths, and the materials in these zones underwent a recrystallization process. Finally, the nanoindentation results revealed inhomogenous mechanical behaviors in the bonding zones, which could be well related to the changes of microstructure and chemical composition.

Key words: explosive welding; tantalum coating; adiabatic shear band; nanoindentation

1 Introduction

Recent trends in the fields of nuclear and chemical industries place high demands on strength and corrosion resistance of advanced structural materials [1]. Since tantalum (Ta) is one of the best corrosion-resistant materials among rare metals and steel owns excellent mechanical properties, the Ta-coated steel plate is an ideal material to address this concern. However, due to the metallurgical incompatibility, thermal physical property mismatch, and formation of intermetallic compounds, fabrication of a high quality Ta coating on Fe substrate using conventional processes remains a challenging task. For instance, the Ta coatings achieved by spraying and overlaying show weaknesses like low strength, thin thickness, and porosity [2−4], which cannot meet the requirements of applications in harsh and aggressive corrosive environments. Explosive welding (EW) of Ta foil with a thickness level of 10^2 μm and steel plate is considered as an alternative method for preparing premium Ta coating. During this process, the explosion energy is used to accelerate a Ta foil towards a stationary steel plate, leading to a high-velocity impact and subsequent formation of metallurgical bond at the Ta/Fe interface [5,6]. Since EW is a solid-state process with an extreme short duration of ~10^{-6} s, it provides competitive advantages of high bonding strength, few melt and ability to keep the thickness even [7,8].

Nevertheless, EW technique is generally used to join two metal plates with a thickness greater than 1 mm, which remains a great technical challenge to foils that have a thickness level of only

Corresponding author: Ming YANG, Tel: +86-15555481852, E-mail: ym1991@njust.edu.cn
DOI: 10.1016/S1003-6326(23)66269-7

10^2 μm. As we know, EW is a harsh thermo-mechanical process involving high temperature, high pressure and complex plastic deformation, which easily induces undesirable defects such as wrinkles, cracks, and voids in the metal foil. Even so, considering the attractive application prospect, many efforts have been made to seek a suitable method that enables to obtain a successful weld without any defects in the foils. HOKAMOTO et al [9] developed an underwater EW assembly to produce a uniform detonation pressure, and thus, a defect-free amorphous foil was successfully coated on Fe substrate. SUN et al [10] also utilized underwater EW technique to join Cu foil and SKS3 steel plate. However, ZHOU et al [11] argued that the underwater EW technique was too complex to have industrial prospects, instead, they placed a buffer layer between the explosive and foil, by which W foils with thicknesses of 0.1−0.5 mm were joined onto Cu plates. Similarly, LIU et al [12] successfully joined glass foil and Al plate by an adjusted EW technique. Recently, we explored an improved EW technique, by which defect-free results have been obtained in works on the welding of Cu foil/Fe [13], Ti foil/Cu [14] and Ag foil/Al [15], which shows a good application prospect.

Although there have been a few successful attempts to fabricate metal coatings by EW, very little attention has been paid to understanding the microstructure related properties at the joint interface. Referring to the EW interface of two metal plates, the most distinctive feature of the joints is the wave structure. In certain circumstance, vortex zone characterized by unique rotational trajectory and intense material mixing, can be found at the crest and trough. Apparently, these large deformations would cause remarkable grain structure changes, such as the formation of amorphous structures [16], nanoscale grains [17,18], intermetallics [19,20], columnar grains [21], and recrystallized grains [22]. As a result, the micro mechanical properties of materials near the interface are changed, and a heterogeneous bonding zone is expected to be formed. However, the microstructure evolution of the EW coated interface is yet to be fully understood. Especially, the effect of the microstructure on mechanical properties remains unclear. We attribute the lack of in-depth understanding on the microstructure related properties, to the difficulties in characterizing such a complex microstructure via conventional metallographic methods.

This work aims to produce a thorough comprehension concerning the metallurgical and mechanical properties of the Ta/Fe interface. For this, a self-developed EW configuration was employed to weld Ta foil and steel plate. The general morphologies and element distributions near the bonding interface were checked by scanning electron microscope (SEM) equipped with energy dispersive spectrometry (EDS) detectors. Electron backscatter diffraction (EBSD) analyses were carried out to reveal the grain changes, and nanoindentation tests were employed to identify micromechanical heterogeneity. This comprehensive study allows further understanding microstructure related properties at the Ta/Fe interface, and providing a guidance for the property optimization and industrial application.

2 Experimental

2.1 Materials and explosive welding procedure

Figure 1 shows the self-developed EW configuration, where an explosive covering cooperated with a buffer structure between the explosive and foil was used to establish an ideal welding condition. Commercial purity Ta foil with dimensions of 150 mm × 80 mm × 0.2 mm was employed as flyer plate, and the base plate was Reduced Activation Ferritic-Martensitic (RAFM) steel with dimensions of 200 mm × 100 mm × 20 mm. This metal combination is of utmost interest to the nuclear fusion industry for its superior resistance to corrosion, and the chemical compositions of the Ta and RAFM steel are given in Tables 1 and 2, respectively. In the initial state,

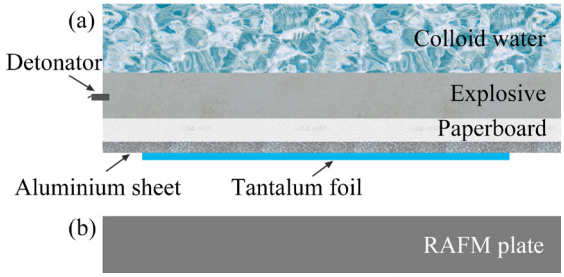

Fig. 1 Schematic of explosive welding of Ta foil (a) and RAFM substrate (b)

the Ta foil was characterized by uniform equiaxed grains with a size of ~10 μm, while the RAFM steel plate was built by typical martensitic structure with a size of ~5 μm. The mechanical properties of Ta foil and RAFM steel plate are given in Table 3. The explosive covering was built by colloid water obtained by mixing 1% highly absorbent polymer and 99% water, which had a density of 0.97 g/cm^3 and thickness of 30 mm. The buffer structure consisted of a paperboard and an aluminum sheet, and both of them were commercially available. The densities of the paperboard and aluminum sheet were 0.36 and 2.7 g/cm^3, and the thicknesses of them were 1 and 2 mm, respectively. The explosive used in this work was emulsion explosive, with a detonation velocity of ~2500 m/s and a density of 0.80 g/cm^3. The stand-off distance between Ta foil and steel plate was set to be 2 mm. All the initial settings established dynamic welding conditions of impact velocity of 435 m/s and collision angle of 10.0°. Details about this configuration and the calculation of dynamic parameters can be found elsewhere [17,23]. It is well established that good welding quality can be accomplished when the dynamic welding conditions are within the range determined by welding window [17]. According to the previous studies [17,23,24], the welding window of Ta to RAFM was developed using collision point velocity v_c and collision angle β. As shown in Fig. 2, it is confirmed that the selected welding parameters are in the middle of the welding window, which suggests that good welding results are expected to be obtained.

2.2 Microstructure and mechanical property analyses

To investigate the interfacial microstructure, a small specimen was extracted by a wire cutting machine from the central parts of the weldment. Then, the specimen was polished by emery papers and micron diamond pastes, successively, where the work cross-section was parallel to the detonation direction. Based on it, a SEM (Gemini500) equipped with EDS probe was used to reveal micro morphology and distribution of chemical element across the interface. For EBSD tests, an argon ion polishing equipment was employed to remove the residual stress from previous processing steps. The EBSD analyses were conducted by accelerating voltage of 20 kV and working distance of 13 mm, and a small step size of only 0.2 μm was selected to display the possible formed ultrafine grains. Finally, the nanoindentation tests were carried out by a consistent loading speed of 500 μN/s and a peak load of 15 mN, with a duration of 5 s at the peak load.

3 Results and discussion

3.1 Interface morphologies

Figure 3(a) shows the SEM image of the Ta/Fe interface, revealing a regular wavy structure with a well-defined amplitude of ~30 μm and period of ~100 μm. It is generally recognized that wave interface is a sign of sound bonding, which enables to improve adhesive strength by increasing bonding area and producing mechanical locking [24,25]. The

Table 1 Chemical composition of Ta (wt.%)

C	N	O	H	Fe	Si	Ti	Ni	Nb	Ta
0.10	<0.10	9.00	0.45	1.5	0.15	0.20	<0.006	<0.02	Bal.

Table 2 Chemical composition of RAFM steel (wt.%)

C	Si	Cr	Mn	W	Ta	V	Ti	N	S	P	Fe
0.10	<0.10	9.00	0.45	1.5	0.15	0.20	<0.006	<0.02	<0.002	<0.003	Bal.

Table 3 Mechanical properties of Ta foil and RAFM steel plate

Material	ρ/(kg·m^{-3})	H_v/MPa	c/(m·s^{-1})	σ_b/MPa	T_m/°C	K/(W·m^{-1}·°C^{-1})	c_p/(J·kg^{-1}·°C^{-1})
Ta	16650	1400	3400	470	2995	54	150
RAFM steel	7850	3000	4500	620	1454	30	446

Note: ρ is the density, H_v is the Vickers hardness, c is the sonic speed, σ_b is the tensile strength, T_m is the melting temperature, K is the thermal conductivity, and c_p is the specific heat capacity

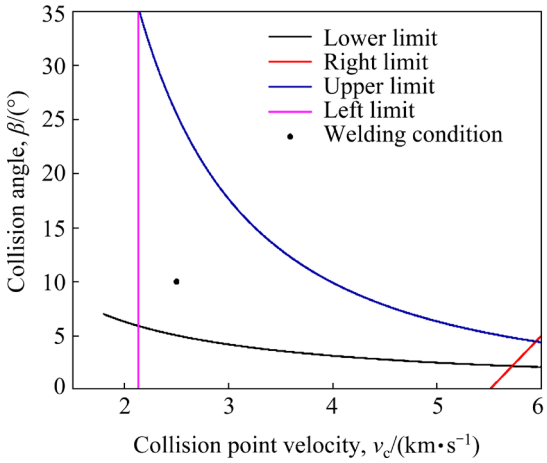

Fig. 2 Ta/RAFM welding window with selected parameter

widely accepted mechanism for the wave formation is the so-called shear instability mechanism, where the high pressure interactions during impact process push the solid metal into a liquid, and then the shear instability flow is initiated by large tangential velocity variations. A detailed explanation about this mechanism can be found in Refs. [26−28]. The enlarged view given in Figs. 3(b−d) indicates that the individual wave is asymmetrical, where Ta matrix is locally elongated and curled into a vortex, while Fe deforms as a whole without any curly trajectory. The asymmetry of the wave is related to the large differences in density and melting point of the two metals [29]. Figures 3(b−d) also reveal the formation of melted zones at the Ta/Fe interface, which mainly concentrate inside the vortex, and occasionally locate at the bonding interface. It should be noted that the formation of a melted zone is a common phenomenon that can be observed in almost all EW systems [30−32]. During the EW process, the high velocity oblique collision induces a severe plastic deformation, friction and shear for interfacial materials, which eventually results in a rapid temperature boost near the bonding interface. According to numerical simulation results, the heating rate of the interfacial materials can reach 10^9 K/s, and the interfacial temperature can even exceed 2000 K, which enables to induce a melt process for most metals [33−35]. The difference between the melted zone observed in this study and previous work is position, where the melted zone for the Ta/Fe weld is bounded within the Ta matrix,

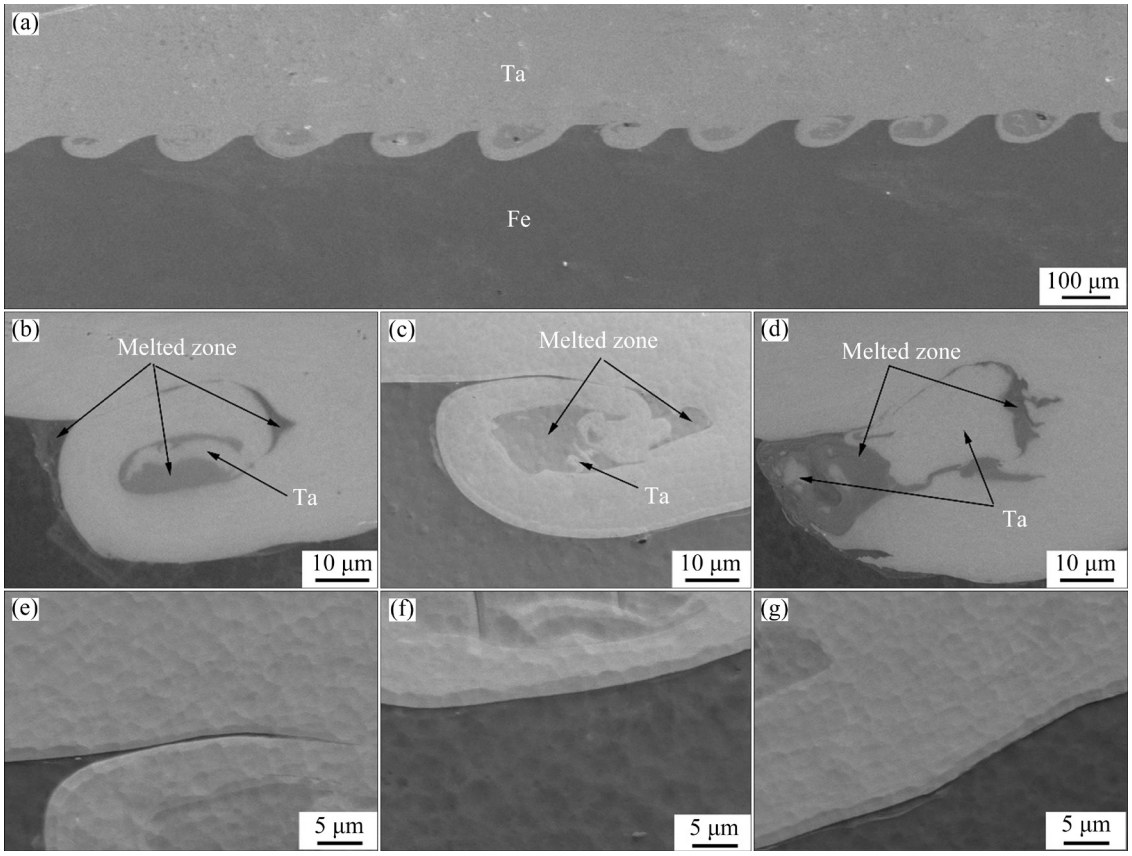

Fig. 3 SEM images of Ta/Fe explosive-welded interfaces: (a) General layout; (b−d) Enlarged view of single wave structure; (e−g) High resolution observation of interface area

while the melted zone is exposed at the bimetallic welded interface for other material combinations like Cu/Fe [36] and Ti/Fe [37]. There are also some Ta fragments enclosed inside the melted zone, which share a random nature with heterogeneous spatial distribution and dispersed shapes. The formation of the Ta fragments could be explained by severe plastic deformation. In this condition, some of Ta matrix began to spall, and the broken Ta fragments traveled into the melted zone along the vortex motion. Unlike the Ta matrix, no visible Fe fragment was found in the melted zone. This could be due to the fact that the Fe element had a lower melting point than Ta, so the Fe matrix was melted under high temperature caused by the plastic deformation. Figures 3(e−g) are the high resolution images showing the different interface areas, where no defects like voids and cracks are found, indicating that a high-quality weld is obtained in this work.

3.2 Element distributions

To give a better understanding of the Ta/Fe interface, EDS analyses were performed focusing on an individual wave, with corresponding results in Fig. 4. Figure 4(a) shows the backscattered electron (BSE) image indicating the test positions, where the varying BSE contrasts are powerful evidences for strong chemical composition changes near the interface. At the right of the vortex (marked by "8"), there is a small mixed zone at the Ta/Fe interface, with a length of 15 μm and a width of 0−5 μm. The interior color of this mixed area is almost uniform, manifesting homogeneous chemical composition. Similar result can be also found in previous work, where a homogeneous melted zone was identified at the Al/Mg EW interface [38]. However, alternating BSE contrasts are observed inside the vortex zone, indicating the heterogeneity of the distribution of chemical elements. By comparing colors, it is deduced that the vortex zone consists of pure Ta fragments and the mixtures of Ta and Fe. This inference is further supported by EDS line scanning result given in Fig. 4(b), where both Ta and Fe elements are detected within the vortex zone. Besides, Fig. 4(b) also shows a sharp transformation of chemical elements across the interface between Ta matrix and the vortex zone, implying that the formation of the vortex zone is governed by intense mechanical mixing of participant metals rather than element diffusion [15]. Figure 4(c) shows the quantitative results of chemical composition obtained by spot scanning, where the average phases of the materials within the vortex zone and at the interfacial mixed zone are determined to be $Ta_{0.63}Fe_{0.37}$ and $Ta_{0.16}Fe_{0.84}$, respectively. The higher percentage of Ta in the vortex zone is probably due to the fact that there are a lot of Ta fragments, while the dominance of Fe in interfacial mixed zone can be explained by its lower melting point. According to the Ta−Fe phase diagram [39], the mixtures of Ta and Fe are easy to form intermetallic compounds at high temperature. During the EW process, the strong mechanical mixing of participating materials together with the high temperature caused by plastic work establishes a favorable condition for the formation of intermetallic compounds. According to the ratio of the elements, it is inferred that these mixed zones contain the intermetallic compounds

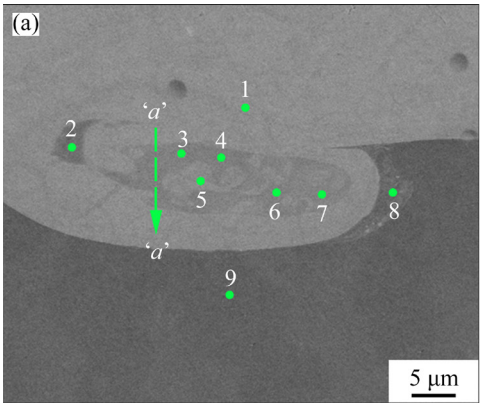

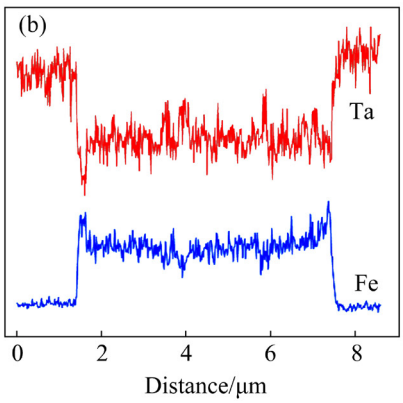

(c)

Position No.	x(Fe)/%	x(Ta)/%
1	0	100.00
2	68.4	31.6
3	40.1	59.9
4	39.2	60.8
5	14.7	85.3
6	56.3	43.7
7	38.4	61.6
8	83.6	16.4
9	100.00	0

Fig. 4 SEM image showing wave structure (a), line scan results (b) across melted zone marked by "*a*-*a*" in (a), and corresponding point scan results (c) with corresponding test regions labeled in (a)

of FeTa and Fe_5Ta_3, which share different mechanical properties with the Ta and Fe matrixes.

3.3 Grain structures

EBSD analyses were carried out to reveal the grain structures of the Ta/Fe interface, with the key results in Figs. 5 and 6. Figure 5(a) shows the inverse pole figure (IPF) with the crystal orientation-color relation map, which indicates the global grain information near the interface. Clearly, the EW process induces a microstructure evolution and leads to formation of a diversity of the metallurgical structures. On Ta side, elongated structures are well visible in the layer adjacent to the interface, with a width of only 1−2 μm and a length up to 10−100 μm. These elongated grains were severely curved along the vortex structures, reflecting very well the rotation characteristics of material displacement during the interface formation. It should be noted that the highly curved grains were typically observed at EW interfaces, referring to the works on welding of Ti/Fe [40], Ta/Cu [1] and Cu/Fe [41], etc. The formation of such a curved grain may be a consequence of strong plastic flow governed by shear instability. The corresponding evidence indicating the large deformation is the inconsistent colors within grain boundaries. For instance, the grain in green color contains blue micro regions, which indicates local orientation changes induced by deformation. Also, there are some fine equiaxed grains inside the vortex, with a size of ~600 nm (Fig. 5(b)). The formation of the fine grains can be explained by ultrahigh temperature in the vortex zone, which induces a dynamic recrystallization process. It should be noted that the interior of the vortex is dominated by black color of low Kikuchi band contrast, indicating that this zone is not or poorly indexed by EBSD tests. This may be due to the disordered arrangement of atoms caused by the

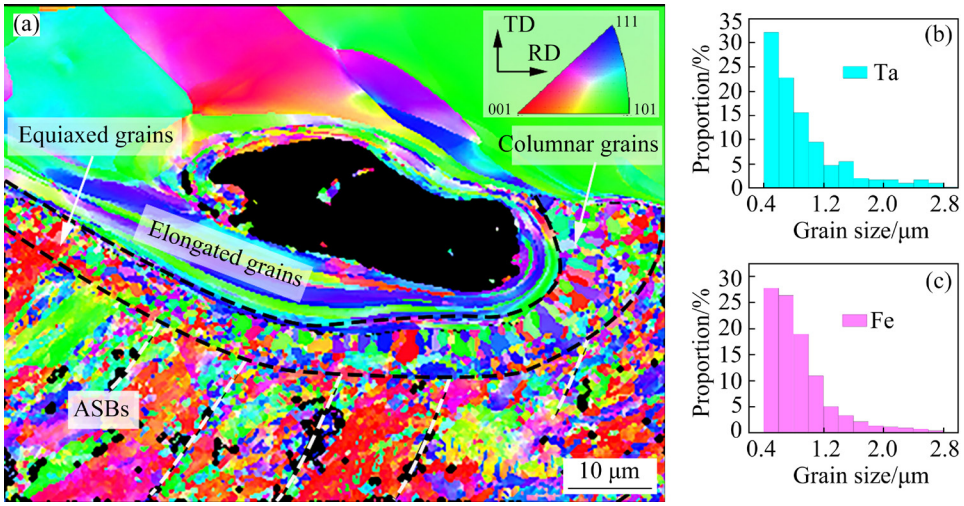

Fig. 5 EBSD IPF combined with crystal orientation-color relation map (a), and grain size distributions of Ta (b) and Fe (c)

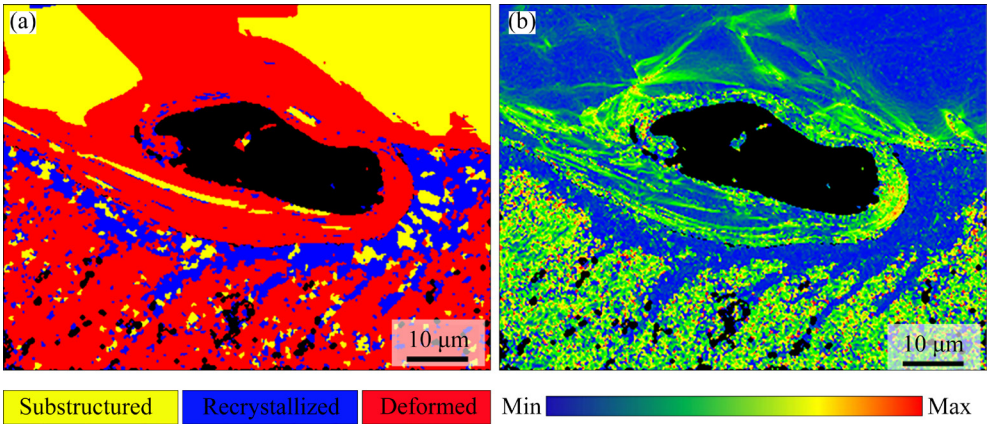

Fig. 6 Recrystallization distribution diagram (a), and KAM map computed from EBSD raw data (b)

severe plastic deformation of the materials, resulting in formation of an amorphous structure and large residual stress in this region. Similar phenomenon can be also found in previous work [42]. Unlike Ta matrix, the Fe matrix adjacent to the interface is built by a fine grain layer with a width of 5−15 μm, as marked by black dotted line in Fig. 5(a). The fine grain layer is heterogeneous. On the left side, the grains are characterized by uniform equiaxed structure with a size of ~500 nm (Fig. 5(c)), which is a typical characteristic of dynamic recrystallization. It is well known that new grains nucleate and grow in the deformed zone when the temperature exceeds ~0.4T_m (T_m is the melting point) [43,44]. According to simulation result, both conditions of high temperature and large plastic strain can be satisfied for the Fe material near the interface [13,15]. On the right side, however, there are many columnar grains with a length of ~5 μm and a width of only ~1 μm. These columnar grains show a growth direction perpendicular to the Ta/Fe interface, which are similar to the metallurgical structures typically observed in conventional fusion welding process, indicating that the materials in this zone experienced melt and re-solidification processes [45]. With the distance slightly away from the interface (close to the fine grain layer), coarse grains with well-defined elongation direction are observed. Meanwhile, there are a large number of small grains, which are imprisoned within the big grains or at the grain boundary. The formation of these features is due to strong plastic deformation favored by shear motion upon the high-speed oblique impact. Especially, there are some small equiaxed grains arranged in strips, which are the typical characteristic of adiabatic shear bands (ASBs), as marked by white dotted line. The formation of the ASBs is a consequence of stress wave concentration, which induces localized adiabatic heating along the narrow paths. As a result, the materials near the ASBs undergo dynamic recovery and recrystallization processes. It is interesting to note that different ASBs are arranged almost in parallel, which indicates the consistent directivity of stress wave.

Figure 6(a) shows the recrystallization distribution diagram, where the recrystallized grains are colored by blue, while the yellow and red represent substructured and deformed grains, respectively. It can be seen from Fig. 6(a) that the Ta matrix is dominated by deformed grains with only a few of recrystallized grains in local region, while abundant recrystallized grains exist in neighborhood of interface in Fe matrix. These features confirm very well the formation mechanisms of different grain structures observed in Fig. 5. In particular, several strips built by recrystallized grains are observed in the locations of ASBs occurring, which provides a strong support for recrystallization processes induced by adiabatic shear in parent metals. Figure 6(b) shows the mapping of kernel average misorientation (KAM), representing the level of plastic deformation. The layer with high dislocation density is detected on Ta side, and the density value decreases with increasing distance from the interface. On Fe side, on the contrary, the region adjacent the interface is characterized by low dislocation density, while the layer with high dislocation density is found slightly away from the interface. This may be due to the recrystallization process that erases the impact-induced dislocations.

3.4 Nanoindentation tests

To correlate the grain changes with the mechanical properties, nanoindentation tests focusing on a typical wave were performed, with corresponding results given in Fig. 7. Figure 7(a) shows the SEM image of the Ta/Fe interface, showing test positions and corresponding nano-hardness values. It is evident from Fig. 7(a) that different materials exhibit different mechanical responses, where an ultrahigh nano-hardness of 17.4 GPa is found for the mixture in the vortex area, which is far higher than the value of Fe and Ta matrixes near the interface. The ultrahigh hardness in the vortex area confirms the result that strong and hard intermetallic compounds like FeTa and Fe_5Ta_3 were formed in this zone, as indicated by EDS analysis. The similar results can be also found in previous works, where ultra-high hardness was detected at the Ti/Fe [46] and Al/Mg EW interfaces [47]. Figure 7(b) shows the typical load−depth curves, where, under the same loading conditions, the indentation depths of Ta, Fe and mixture are found to be 500, 450 and 300 nm, respectively. In addition, Fig. 7 also reveals that the same materials in different positions have varying hardness values. For example, the hardness of Ta

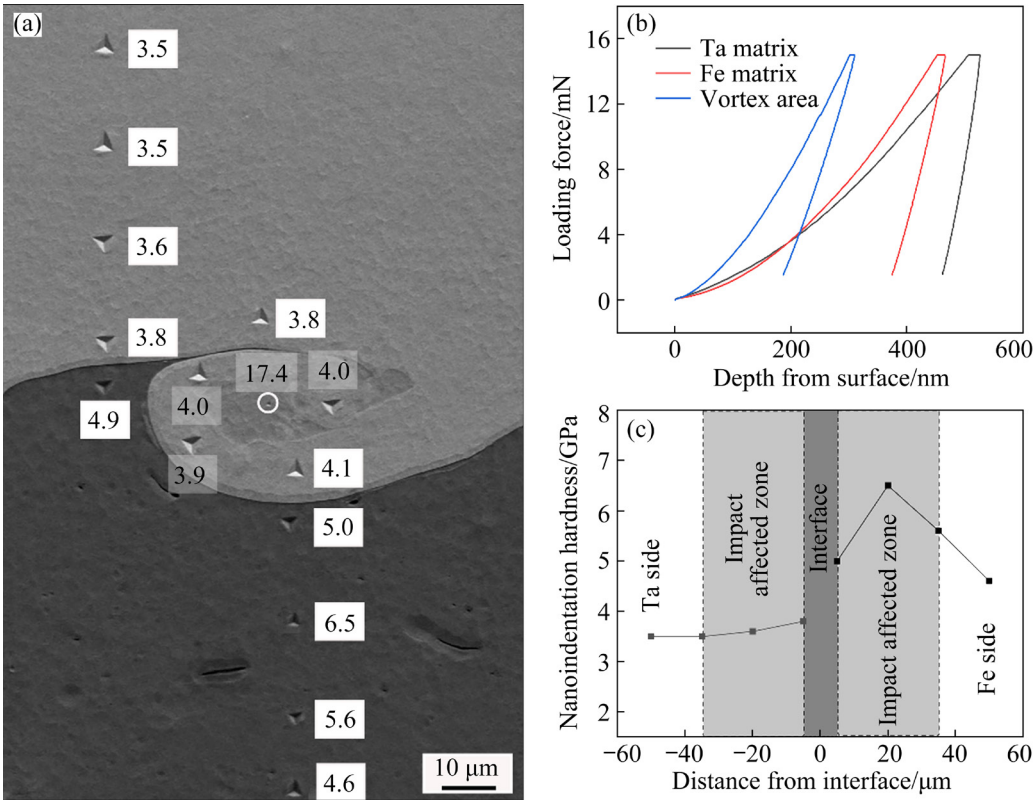

Fig. 7 Nanoindentation test results at Ta/Fe interface: (a) SEM image showing indentation test regions and corresponding nano-hardness values; (b) Typical load–depth curves of different materials; (c) Nanoindentation hardness variation across interface

matrix at the vortex boundary is slightly higher than that near the interface, due to higher degree of work hardening near the vortex zone. Figure 7(c) shows the variation of hardness across the Ta/Fe interface, which reveals higher levels of hardness values for the materials near the interface, and the width of the high hardness zone is determined to be about 40 μm on both sides of the interface. According to EBSD results in Fig. 5, the distribution of hardness value is related to grain structure changes induced by EW process. In Ta matrix, the grains near the interface are elongated and refined in local area, while Fe matrix near the interface is dominated by newly formed fined grains. It is evident that these grain structure changes would lead to the increase in grain boundary area. As a result, the resistance to a compressive force during nanoindentation measurements is expected to increase. It should be noted that, in Fe matrix, the region in the proximity of the interface shows a lower hardness when compared to the region slightly away from the interface, but still higher than the original value. This may be due to the fact that the materials in this region undergo a recrystallization process, which has a thermal softening effect.

4 Conclusions

(1) The EW technique is found to be an effective way to fabricate Ta foil/steel composite, where the obtained joint shows regular wavy structures with a well-defined amplitude of ~30 μm and a period of ~100 μm, and no defects like voids and cracks are found in the bonding zone.

(2) The melted zones are mainly observed within the vortex structures, and occasionally at the Ta/Fe interfaces, and the SEM/EDS analyses reveal that vortex melted zones consist of pure Ta fragments and the mixtures of Ta and Fe.

(3) EBSD analyses reveal a diversity of the grain structures near the Ta/Fe interface. In Ta matrix, the grains are elongated and severely curved along the vortex structures, while the Fe matrix adjacent to the interface is built by extra fine recrystallized grains with two types of structures (equiaxed and columnar shapes). Especially, several ASBs are

found in Fe matrix slightly away from the interface, which are filled with small equiaxed grains.

(4) The nanoindentation results show inhomogenous mechanical behaviors for materials near the interface. In Ta matrix, the hardness values decrease with increasing distance from the interface, while the Fe matrix shows a trend of first increase and then decrease. In particular, an ultrahigh hardness of 17.4 GPa is detected in the vortex area, which comfirms the formation of intermetallic compounds.

Acknowledgments

The research is supported by the National Natural Science Foundation for Young Scientists of China (Nos. 12102427, 12102202).

References

[1] PAUL H, CHULIST R, LITYŃSKA-DOBRZYŃSKA L, PRAŻMOWSKI M, FARYNA M, MANIA I, SZULC Z, MISZCZYK M M, KUREK A. Interfacial reactions and microstructure related properties of explosively welded tantalum and steel sheets with copper interlayer [J]. Materials & Design, 2021, 208: 109873.

[2] WEI D B, CHEN X H, ZHANG P Z, DING F, LI F K, YAO Z J. Plasma surface tantalum alloying on titanium and its corrosion behavior in sulfuric acid and hydrochloric acid [J]. Applied Surface Science, 2018, 441: 448−457.

[3] GLADCZUK L, PATEL A, PAUR C S, SOSNOWSKI M. Tantalum films for protective coatings of steel [J]. Thin Solid Films, 2004, 467: 150−157.

[4] MAENG S, AXE L, TYSON T A, GLADCZUK L, SOSNOWSKI M. Corrosion behaviour of magnetron sputtered α- and β-Ta coatings on AISI 4340 steel as a function of coating thickness [J]. Corrosion Science, 2006, 48: 2154−2171.

[5] POURALIAKBAR H, KHALAJ G, JANDAGHI M R, FADAEI A, GHAREH-SHIRAN M K, SHIM S H, HONG S I. Three-layered SS321/AA1050/AA5083 explosive welds: Effect of PWHT on the interface evolution and its mechanical strength [J]. International Journal of Pressure Vessels and Piping, 2020, 188: 104216.

[6] SHIRAN M K G, KHALAJ G, POURALIAKBAR H, JANDAGHI M R, DEHNAVI A S, BAKHTIARI H. Multilayer Cu/Al/Cu explosive welded joints: Characterizing heat treatment effect on the interface microstructure and mechanical properties [J]. Journal of Manufacturing Processes, 2018, 35: 657−663.

[7] ACARER M, GÜLEÇ B, FINDIK F. The influence of some factors on steel/steel bonding quality on there characteristics of explosive welding joints [J]. Journal of Materials Science, 2004, 39: 6457−6466.

[8] CORIGLIANO P, CRUPI V, GUGLIELMINO E. Non linear finite element simulation of explosive welded joints of dissimilar metals for shipbuilding applications [J]. Ocean Engineering, 2018, 160: 346−353.

[9] HOKAMOTO K, NAKATA K, MORI A, TSUDA S, TSUMURA T, INOUE A. Dissimilar material welding of rapidly solidified foil and stainless steel plate using underwater explosive welding technique [J]. Journal of Alloys and Compounds, 2009, 472: 507−511.

[10] SUN Wei, LI Xiao-jie, YAN Hong-hao, HOKAMOTO K. Effect of initial hardness on interfacial features in underwater explosive welding of tool steel SKS_3 [J]. Journal of Materials Engineering and Performance. 2014, 23: 421−428.

[11] ZHOU Qiang, FENG Jian-rui, CHEN Peng-wan. Numerical and experimental studies on the explosive welding of tungsten foil to copper [J]. Materials, 2017, 10: 984.

[12] LIU W D, LIU K X, CHEN Q Y, WANG J T, YAN H H, LI X J. Metallic glass coating on metals plate by adjusted explosive welding technique [J]. Applied Surface Science, 2009, 255: 9343−9347.

[13] YANG Ming, XU Jun-feng, MA Hong-hao, LEI Ming-zhun, NI Xiao-jun, SHEN Zhao-wu. ZHANG B Y, TIAN J. Microstructure development during explosive welding of metal foil: Morphologies, mechanical behaviors and mechanisms [J]. Composites Part B: Engineering, 2021, 212: 108685.

[14] XU Jun-feng, YANG Ming, CHEN Dai-guo, MA Hong-hao, SHEN Zhao-wu, ZHANG Bing-yuan, TIAN Jie. Providing a new perspective for obtaining high-quality metal coatings: Fabrication and properties studies of TA2 foil on Q235 steel by explosive welding [J]. Archives of Civil and Mechanical Engineering, 2021, 21: 1−11.

[15] YANG Ming, XU Jun-feng, CHEN Dai-guo, MA Hong-hao, SHEN Zhao-wu, ZHANG Bing-yuan, TIAN Jie. Understanding interface evolution during explosive welding of silver foil and Q235 substrate through experimental observation coupled with simulation [J]. Applied Surface Science, 2021, 566: 150703.

[16] PAUL H, MORGIEL J, BAUDIN T, BRISSET F, PRAŻMOWSKI M, MISZCZYK M. Characterization of explosive weld joints by TEM and SEM/EBSD [J]. Archives of Metallurgy and Materials, 2014, 59: 1129−1136.

[17] YANG Ming, MA Hong-hao, SHEN Zhao-wu, HUANG Ze-Chun, TIAN Qi-Chao, TIAN Jie. Dissimilar material welding of tantalum foil and Q235 steel plate using improved explosive welding technique [J]. Materials & Design, 2020, 186: 108348.

[18] FRONCZEK D M, WOJEWODA-BUDKA J, CHULIST R, SYPIEN A, KORNEVA A, SZULC Z, SCHELL N, ZIEBA P. Structural properties of Ti/Al clads manufactured by explosive welding and annealing [J]. Materials & Design, 2016, 91: 80−89.

[19] YANG Ming, MA Hong-hao, SHEN Zhao-wu, CHENG Dai-guo, DENG Yong-xin. Microstructure and mechanical properties of Al−Fe meshing bonding interfaces manufactured by explosive welding [J]. Transactions of Nonferrous Metals Society of China, 2019, 29: 680−691.

[20] CARVALHO G H S F L, GALVÃO I, MENDES R, LEAL R M, LOUREIRO A. Explosive welding of aluminium to stainless steel using carbon steel and niobium interlayers [J]. Journal of Materials Processing Technology, 2020, 283: 116707.

[21] PAUL H, MISZCZYK M M, CHULIST R, PRAŻMOWSKI M, MORGIEL J, GAŁKA A, FARYNA M, BRISSET F. Microstructure and phase constitution in the bonding zone of explosively welded tantalum and stainless steel sheets [J]. Materials & Design, 2018, 153: 177−189.

[22] ZHANG Heng, JIAO Ke-xin, ZHANG Jian-liang, LIU Jian-ping. Microstructure and mechanical properties investigations of copper-steel composite fabricated by explosive welding [J]. Materials Science and Engineering: A, 2018, 731: 278−287.

[23] YANG Ming, MA Hong-hao, SHEN Zhao-wu. Study on self-restrained explosive welding with high energy efficiency [J]. The International Journal of Advanced Manufacturing Technology, 2018, 99: 3123−3132.

[24] YANG Ming, MA Hong-hao, SHEN Zhao-wu, SUN Yu-ling. Study on explosive welding for manufacturing meshing bonding interface of CuCrZr to 316L stainless steel [J]. Fusion Engineering and Design, 2019, 143: 106−114.

[25] SONG J, KOSTKA A, VEEHMAYER M, RAABE D. Hierarchical microstructure of explosive joints: Example of titanium to steel cladding [J]. Materials Science and Engineering: A, 2011, 528: 2641−2647.

[26] NASSIRI A, KINSEY B, CHINI G. Shear instability of plastically-deforming metals in high-velocity impact welding [J]. Journal of the Mechanics and Physics of Solids, 2016, 95: 351−373.

[27] BEN-ARTZY A, STERN A, FRAGE N, SHRIBMAN V, SADOT O. Wave formation mechanism in magnetic pulse welding [J]. International Journal of Impact Engineering, 2010, 37: 397−404.

[28] ROBINSON J L. The mechanics of wave formation in impact welding [J]. Philosophical Magazine, 1975, 31: 587−597.

[29] DURGUTLU A, OKUYUCU H, GULENC B. Investigation of effect of the stand-off distance on interface characteristics of explosively welded copper and stainless steel [J]. Materials & Design, 2008, 29: 1480−1484.

[30] SARAVANAN S, RAGHUKANDAN K. Microstructure, strength and welding window of aluminum alloy−stainless steel explosive cladding with different interlayers [J]. Transactions of Nonferrous Metals Society of China, 2022, 32: 91−103.

[31] CHU Qiao-ling, XIA Tuo, ZHAO Peng-kang, ZHANG Min, ZHENG Jian-ming, YAN Fu-xue, CHENG Peng, YAN Cheng, LIU Chuan, LUO Hai-long. Interfacial investigation of explosion-welded Al/steel plate: The microstructure, mechanical properties and residual stresses [J]. Materials Science and Engineering: A, 2022, 833: 142525.

[32] ZHOU Qiang, LIU Rui, ZHOU Qiang, RAN Chun, FAN Ke-she, XIE Jing, CHEN Peng-wan. Effect of microstructure on mechanical properties of titanium-steel explosive welding interface [J]. Materials Science and Engineering: A, 2022, 830: 142260.

[33] BATAEV I A, LAZURENKO D V, TANAKA S, HOKAMOTO K, BATAEV A A, GUO Y, JORGE A M Jr. High cooling rates and metastable phases at the interfaces of explosively welded materials [J]. Acta Materialia, 2017, 135: 277−289.

[34] NASSIRI A, ABKE T, DAEHN G. Investigation of melting phenomena in solid-state welding processes [J]. Scripta Materialia, 2019, 168: 61−66.

[35] BATAEV I A, TANAKA S, ZHOU Qiang, LAZURENKO D V, JORGE A M Jr, BATAEV A A, HOKAMOTO K, MORI A, CHEN Peng-wan. Towards better understanding of explosive welding by combination of numerical simulation and experimental study [J]. Materials & Design, 2019, 169: 107649.

[36] ZHANG Heng, JIAO Ke-xin, ZHANG Jian-liang, LIU Jian-ping. Comparisons of the microstructures and micro-mechanical properties of copper/steel explosive-bonded wave interfaces [J]. Materials Science and Engineering: A, 2019, 756: 430−441.

[37] GLOC M, WACHOWSKI M, PLOCINSKI T, KURZYDLOWSKI K J. Microstructural and microanalysis investigations of bond titanium grade1/low alloy steel st52-3N obtained by explosive welding [J]. Journal of Alloys and Compounds, 2016, 671: 446−451.

[38] ZHANG Ting-ting, WANG Wen-xian, ZHANG Wei, WEI Yi, CAO Xiao-qing, YAN Zhi-feng, ZHOU Jun. Microstructure evolution and mechanical properties of an AA6061/AZ31B alloy plate fabricated by explosive welding [J]. Journal of Alloys and Compounds, 2018, 735: 1759−1768.

[39] HIROAKI OKAMOTO. ASM Hand Book [M]. Materials Park: ASM International, 1992.

[40] CHU Qiao-ling, ZHANG Min, LI Ji-hong, YAN Chen. Experimental and numerical investigation of microstructure and mechanical behavior of titanium/steel interfaces prepared by explosive welding [J]. Materials Science and Engineering: A, 2017, 689: 323−331.

[41] YANG Ming, MA Hong-hao, YAO Da-mao, SHEN Zhao-wu. Experimental study for manufacturing 316L/CuCrZr hollow structural component [J]. Fusion Engineering and Design, 2019, 144: 107−118.

[42] ZHANG Wen-tao, XIE Ji-lin, CHEN Yu-hua, ZHANG Li-ping, YIN Li-meng, ZHANG Ti-ming, WANG Shan-lin. Interfacial microstructure and bonding mechanism of the Al/Ti joint by magnetic pulse welding [J]. Scripta Materialia, 2022, 210: 114434.

[43] SHA Y H, SUN C, ZHANG F, PATEL D, CHEN X, KALIDINDI S R, ZUO L. Strong cube recrystallization texture in silicon steel by twin-roll casting process [J]. Acta Materialia, 2014, 76: 106−117.

[44] JONAS J J, QUELENNEC X, JIANG L, MARTIN É. The Avrami kinetics of dynamic recrystallization [J]. Acta Materialia, 2009, 57: 2748−2756.

[45] LEE T, NASSIRI A, DITTRICH T, VIVEK A, DAEHN G. Microstructure development in impact welding of a model system [J]. Scripta Materialia, 2020, 178: 203−206.

[46] ROSENTHAL I, MIRIYEV A, TUVAL E, STERN A, FRAGE N. Characterization of explosion-bonded Ti-alloy/steel plate with Ni interlayer [J]. Metallography Microstructure and Analysis, 2014, 3: 97−103.

[47] VENKATESWARAN P, XU Zhi-hui, LI Xiao-dong, REYNOLDS A P. Determination of mechanical properties of Al−Mg alloys dissimilar friction stir welded interface by indentation methods [J]. Journal of Materials Science, 2009, 44: 4140−4147.

钽箔/钢板爆炸复合界面的显微组织与力学性能

杨 明，王金相

南京理工大学 瞬态物理国家重点实验室，南京 210094

摘 要：为加深对爆炸复合界面微观性能的理解，采用自主研发的爆炸焊接技术制备钽箔/钢板复合试样，通过不同的表征方法对其界面显微组织和力学性能进行研究。结果表明，钽/钢界面呈现波长和波幅分布均匀的波形结构。熔化区主要位于涡旋内部，只有少量分布在结合界面处，其形成原因是由于两种金属强烈的机械混合。电子背散射实验揭示了钽/钢界面存在多样性的晶体结构，在钽中形成高度弯曲和细长晶粒，而钢中形成细小的等轴晶和柱状晶粒。在钢中发现了多条由小等轴晶组成的绝热剪切带，这是由于应力波集中在狭窄的路径中，导致该区域内的材料发生再结晶过程。纳米压痕结果揭示了结合区域不均匀的力学性能，很好地证明了碰撞诱导的显微组织和化学成分变化。

关键词：爆炸焊接；钽涂层；绝热剪切带；纳米压痕

(Edited by Xiang-qun LI)